Published in final edited form as:
Oral Oncol. 2012 August ; 48(8): 717–722. doi:10.1016/j.oraloncology.2012.02.001.

Correlation of a priori DCE-MRI and ^{1}H-MRS data with molecular markers in neck nodal metastases: Initial analysis

Jacobus F.A. Jansen, Ph.D.[1,2,5], **Diane L. Carlson, M.D.**[3,6], **Yonggang Lu, Ph.D.**[1,2], **Hilda. E. Stambuk, M.D.**[2], **Andre L. Moreira, M.D., Ph.D.**[3], **Bhuvanesh Singh, M.D., Ph.D., FACS**[4], **Snehal G. Patel, M.D., FACS**[4], **Dennis H. Kraus, M.D., FACS**[4], **Richard J. Wong, M.D., FACS**[4], **Ashok R. Shaha, M.D., FACS**[4], **Jatin P. Shah, M.D., FACS**[4], and **Amita Shukla-Dave, Ph.D.**[1,2]

[1]Department of Medical Physics, Memorial Sloan-Kettering Cancer Center, New York, NY

[2]Department of Radiology, Memorial Sloan-Kettering Cancer Center, New York, NY

[3]Department of Pathology, Memorial Sloan-Kettering Cancer Center, New York, NY

[4]Department of Surgery, Memorial Sloan-Kettering Cancer Center, New York, NY

Abstract

Objectives—The aim of the present study is to correlate non-invasive, pretreatment biological imaging (dynamic contrast enhanced-MRI [DCE-MRI] and proton magnetic resonance spectroscopy [^{1}H-MRS]) findings with specific molecular marker data in neck nodal metastases of head and neck squamous cell carcinoma (HNSCC) patients.

Materials and Methods—Pretreatment DCE-MRI and ^{1}H-MRS were performed on neck nodal metastases of 12 patients who underwent surgery. Surgical specimens were analyzed with immunohistochemistry (IHC) assays for: Ki-67 (reflecting cellular proliferation), vascular endothelial growth factor (VEGF) (the “endogenous marker” of tumor vessel growth), carbonic anhydrase (CAIX), hypoxia inducible transcription factor (HIF-1α), and human papillomavirus (HPV). Additionally, necrosis was estimated based on H&E staining. The Spearman correlation was used to compare DCE-MRI, ^{1}H-MRS, and molecular marker data.

Results—A significant correlation was observed between DCE-MRI parameter std(k_{ep}) and VEGF IHC expression level (rho = 0.81, p = 0.0001). Furthermore, IHC expression levels of Ki-67 inversely correlated with std(K^{trans}) and std(v_e) (rho = −0.71; p = 0.004, and rho = −0.73; p = 0.003, respectively). Other DCE-MRI, ^{1}H-MRS and IHC values did not show significant correlation.

Conclusion—The results of this preliminary study indicate that the level of heterogeneity of perfusion in metastatic HNSCC seems positively correlated with angiogenesis, and inversely correlated with proliferation. These results are preliminary in nature and are indicative, and not

Corresponding author: Amita Shukla-Dave, Ph.D., Department of Medical Physics & Radiology, Memorial Sloan-Kettering Cancer Center, 1275 York Avenue, Box 84, New York, New York 10065, Telephone: 212.639.3184, Fax: 212.717.3010, davea@mskcc.org.
[5]Present address: Department of Radiology, Maastricht University Medical Center, Maastricht, The Netherlands.
[6]Present address: Department of Laboratory Medicine and Pathology, Cleveland Clinic Florida, Weston, Florida.

Portions of the results were presented as abstract 2824 at the International Society for Magnetic Resonance in Medicine - European Society for Magnetic Resonance in Medicine and Biology Joint Annual Meeting in Stockholm, Sweden, May 6th, 2010.

definitive, trends portrayed in HNSCC patients with nodal disease. Future studies with larger patient populations need to be carried out to validate and clarify our preliminary findings.

Keywords

Head and neck squamous cell carcinoma; ^{1}H-MRS; DCE-MRI; molecular markers

Introduction

Head and neck squamous cell carcinoma (HNSCC) is the most common type of head and neck cancer in the United States.[1] Despite recent advances in surgical and oncologic treatments, the survival rate of patients with HNSCC has not changed over the past decade; the 5-year and 10-year relative survival rates are 61% and 50% respectively.[1] Non-invasive imaging and molecular markers have a potential role in clinical decision-making for patients with head and neck (HN) cancer, but patient and treatment heterogeneity prohibits definitive conclusions.[2, 3] Therefore, the precise role of the clinical application of molecular prognostic markers in HN cancers remains elusive.[2, 4]

One promising noninvasive imaging modality is magnetic resonance imaging (MRI). Pharmacokinetic modeling of the dynamic contrast-enhanced magnetic resonance imaging (DCE-MRI) data yields physiologic parameters relevant for functional characterization of changes in tumor microvasculature.[5] In contrast to conventional MRI techniques, which only allow qualitative characterization of tumor, the pharmacokinetic modeling of DCE-MRI data provides functional information about the tumor. Another MRI-based technique is proton magnetic resonance spectroscopy (^{1}H-MRS), which provides a window on the metabolite composition of tumors.[6] For example, ^{1}H-MRS enables detection of choline-containing compounds, which reflect membrane synthesis and indirectly elevated cell proliferation rates.

A quantitative estimate of tumor microenvironment parameters can also be obtained through immunohistochemistry (IHC) assays.[2] For example, hypoxia and proliferation levels have been shown to be relevant for treatment outcome. These levels have been evaluated for malignant progression and prediction or monitoring of response to treatment.[7–9] Several prognostic molecular markers have been identified in HN cancers.[8, 10] These markers include Ki-67 (reflecting cellular proliferation), VEGF (vascular endothelial growth factor; the “endogenous marker” of tumor vessel growth), carbonic anhydrase (CAIX), hypoxia inducible transcription factor (HIF-1α), and human papillomavirus (HPV). The objective of this study is to correlate non-invasive, pretreatment biological MR imaging (DCE-MRI and ^{1}H-MRS) findings with specific molecular marker data in neck nodal metastases of HNSCC patients. This may provide information that could improve the clinical interpretation of *in vivo* MRI data and allow the development of “patterns” that might enable physicians to provide patient-specific treatment.

Patients and Methods

Our study was approved by the Institutional Review Board and was compliant with the Health Insurance Portability and Accountability Act. Inclusion criteria for the study were as follows: biopsy-proven squamous cell carcinoma; presence of nodal metastasis in the neck; ability to give informed consent; no contraindications to MRI. After giving informed consent, 46 patients were enrolled in our prospective MRI study from March 2006 to March 2008 (Figure 1). Of these, 12 patients had surgery. Thus, our study included 12 patients (4 females and 8 males, with an average age of 57±13 years (mean ± SD)). The patients’ primary tumor locations were as follows: base of tongue (2), tonsil (2), oral tongue (1), hard

palate (1), buccal mucosa (2), and unknown (4). The clinical characteristics of all patients analyzed in the study are summarized in Table 1.

MRI studies: ^{1}H-MRS and DCE-MRI

Pretreatment MRI data from all 12 patients were acquired on a 1.5 Tesla G.E. Excite scanner (General Electric, Milwaukee, WI) with a 4-channel neurovascular phased-array coil. MR imaging covering the entire neck was performed, as described previously.[11–14] The neck MR imaging protocol consisted of rapid scout images, multiplanar (axial, coronal and sagittal) T2-weighted, fat-suppressed, fast-spin echo images, and multi-planar T1-weighted images. During ^{1}H-MRS, spectra were acquired for the tumor identified on T2-weighted images by a neuro-radiologist, and a volume of interest (>8mL) was placed over the node, using TE (echo time) 136 ms, TR (repetition time) 1.6 s, and 256 averages. Localization and water suppression were achieved with point-resolved spatially localized spectroscopy (PRESS) and chemical shift selective suppression, respectively. A spectrum (16 averages) of unsuppressed water was also recorded. Proton density (PD) images were acquired on the same node studied by ^{1}H-MRS to determine the longitudinal relaxation rate constant R_1 for each DCE-MRI data point in the axial plane. The acquisition parameters for the PD images were as follows: TR of 350 ms, TE of 2 ms with a 30° flip angle (α), 2 excitations, 15.63-kHz receive bandwidth, 18–20–cm field of view, 5–6–mm slice thickness, zero gap and a 256 × 128 matrix. DCE-MRI was acquired using a fast multi-phase spoiled gradient echo sequence. Antecubital vein catheters delivered a bolus of 0.1 mmol/kg Gd-DTPA (Magnevist; Berlex Laboratories, Wayne, NJ) at 2 cc/s, followed by a saline flush. The entire node was covered contiguously with 5–7–mm thick slices with zero gap, yielding 3–8 slices with 3.75–7.5–sec temporal resolution. Acquisition parameters for DCE-MRI were similar to those for PD imaging, except that the TR was 9 ms and 40–80 time course data points were collected. For both PD images and DCE-MRI the 256 × 128 matrix was zero filled to 256 × 256 during image reconstruction.

Planning

To ensure the matching of the node of interest to the surgical node, the following steps were taken by the team of the radiologist, physicist, pathologist and surgeon: i) the neuroradiologist marked the relevant MR images with the node of interest, provided the multiplanar images pre- and post- contrast with the exact location (level) of the node to the physicist, and showed the MR images to the surgeon on picture archiving and communication system (PACS) before the surgery; ii) the physicist helped make a template that was given to the surgeon, and iii) the surgeon used the above information and labeled the node of interest after resection for appropriate identification and orientation, and gave the specimen and copy of the image to the pathologist.

Immunohistochemistry

Following guidelines established by the Institutional Review Board at our institution, fresh tissue samples were sequentially collected under the supervision of the pathologist after obtaining written informed consent from the patients undergoing therapeutic surgical resection for HNSCC by the Head and Neck Service surgeons at our institution from March 2006 to March 2008. In each case, the portion of tumor was resected near the advancing edge of the tumor to avoid its necrotic center. Histologically normal mucosae of the upper aerodigestive tract, resected 5 cm away from the tumor area, were obtained in all cases and used as controls. Paraffin-embedded tissue blocks were obtained for each surgically resected specimen by sectioning each tumor with reference to the plane of imaging of the corresponding preoperative MRI. A sample of the tissue was immediately snap-frozen and stored in liquid nitrogen for further use. Histological sections (4 μm) were obtained from each paraffin-embedded tissue block, and placed onto poly-L-lysine-coated glass slides in

preparation for immunohistochemical stains using antibodies for VEGF, Ki-67, CA-IX, HIF-1α, HPV, and routine hematoxylin and eosin (H&E) staining. Expression levels of VEGF were analyzed using the anti-VEGF mAb, obtained from Santa Cruz, using the Discovery XT (Ventana) with a dilution of 1:100. Ki-67 was analyzed using anti-Ki-67 mAb (Dako), at the Discovery XT (Ventana) with a dilution of 1:100. For CA-IX, a homemade mAb was used, which was performed with heat-induced epitope retrieval in a Citrate buffer for 30′. The dilution of the primary Ab was 1:100, with an overnight incubation at 4°C. The secondary mAb (Vector Laboratories, dilution 1:500) was kept for 1 hour at room temperature in Strepavidin (Dako), with a dilution of 1:500, and 1 hour at room temperature in DAB-5. HIF-1α sections were incubated at 95 °C for 45 min with anti-HIF-1α mAb (Novus Biologicals) at a dilution:1:1600 using the catalyzed signal amplification system from Dako. H&E was completed with hematoxylin solutions for nuclear staining and eosin solutions for cytoplasmic staining (Dako). HPV staining was performed on an automated stainer using INFORM HPV III family 16 probe (Ventana Medical System, Tucson AZ) according to manufacturer instructions. The probe has affinities to HPV genotypes 16, 18, 31, 33, 39, 45, 51, 52, 56, 58, and 66. Adequate positive and negative control slides were included in each batch.

Image Analysis

For each patient, imaging findings from ^{1}H-MRS, DCE-MRI and IHC were analyzed for the largest of the metastatic nodes identified by the neuroradiologist on T2-weighted MR imaging.

^{1}H-MRS and DCE-MRI Analyses—The ^{1}H-MRS spectra were analyzed using the LCModel software package (Version 6.2-1L).[15] The metabolite basis set (PRESS, TE 136 ms, 1.5 T) included simulated macromolecule peaks. For each spectrum, the parts per million (ppm) range included for analysis was 2.7 to 3.8 ppm. The ‘only-cho-2’ setting was used, which provides concentration estimates for choline (Cho) in arbitrary units, relative to water (Cho/W). No corrections for relaxation were performed. The Cramer-Rao lower bound (CRLB), which simultaneously accounts for both resolution and noise level,[16] was calculated as an estimate of the error in metabolite quantification.[17] Metabolite estimates were excluded from analysis if the CRLB exceeded the 50% range.[18]

DCE-MRI data were analyzed with Matlab version R2008. For the tumor tissue time course data, regions of interest (ROIs) were manually drawn by an experienced (> 10 yrs of experience) neuro-radiologist. Each ROI encompassed a whole metastatic node. The same nodes assessed with ^{1}H-MRS were assessed by DCE-MRI. All the slices containing each node were outlined and analyzed. The total number of pixels within the entire ROI was converted into the tumor volume (mm^3). Quantitative DCE-MRI analyses of the tumor tissue time course data was performed using the two-compartment Tofts model in all ROIs.[19] A population-based arterial input function derived from the carotid arteries in head and neck patients was used.[20] The model fitted the tissue contrast agent concentration and yielded quantitative parameters K^{trans} (volume transfer constant in min^{-1}), v_e (volume fraction of the extravascular extracellular space (EES) which is dimensionless), and k_{ep} (rate constant in min^{-1}, which equals the ratio K^{trans}/v_e). DCE-MRI analyses of the tumor tissue were performed on a pixel-by-pixel basis. A histogram analysis was performed on all pixels within the ROI, which yielded the median and standard deviation (std) of the distribution of all pixels. Histograms were normalized to the total number of tumor voxels to allow direct comparisons between patients. The standard deviation describes the width of the distribution and is indicative of the heterogeneity of the tumor.[21]

IHC Analyses—The IHC results for VEGF, Ki-67, CA-9, and HIF-1α were classified by an experienced pathologist (>10 yrs of experience) on an ordinal scale as follows: (−) no staining; (+) immunostaining is less than 1% of cells; (++) immunostaining in 1–10% of cells; (+++) immunostaining in 10–50% of cells; (++++) immunostaining in more than 50% of cells, according to Zhong, et al.[22] Additionally, based on the H&E staining, a percentage of necrosis was estimated (0–100%). Finally, for HPV a dichotomous score was used: (0) no immunostaining, and (1) positive immunostaining when there was specific staining of tumor-cell nuclei for HPV in the analysis.

Statistical Analysis

All statistical calculations were performed using the software SPSS 15.0 for Windows. Inter-modality correlations between ^{1}H-MRS (Cho/W), DCE-MRI (median(K^{trans}), std(K^{trans}), median(v_e), std(v_e), median(k_{ep}), and std(k_{ep})), IHC staining values of VEGF, Ki-67, CA-9, and HIF-1α, necrosis percentages, and tumor volume were calculated using nonparametric Spearman rank correlation. The correlations were interpreted using the guidelines from Cohen, et al.,[23] with absolute correlations of <0.3 considered weak, 0.3–05 considered moderate, and 0.5–1.0 considered strong. Additionally a non-parametric Mann-Whitney U test was performed on the nominal MRI parameters, divided into two groups, based on the dichotomous HPV score. Correlations with a $p < 0.01$ were considered significant. To correct for multiple comparisons, a Bonferroni correction (N=64) was applied.

Results

Out of the 12 HNSCC patients, 7 patients had valid ^{1}H-MRS data, with a median CRLB value for Cho/W of 17 (range, 6 to 26), and an average mean voxel size of 8.1 ± 3.6 ml (mean ± SD). For DCE-MRI, all 12 patients had valid data; for 10 patients 1 node was studied, and for 2 patients 2 nodes were studied, which resulted in a total of 14 nodes. All 14 nodes had valid IHC data for VEGF, Ki-67, CA-9, HIF-1α, HPV and H&E. Out of the 14 nodes, 3 were positive, and 11 were negative for HPV.

Figure 2 displays typical images obtained during the pre-treatment DCE-MRI exam of the neck region of a patient with HNSCC (male, 44 y, primary tonsil). Figure 3 shows the IHC assay results of the corresponding surgical specimen (neck nodal metastases).

Correlations

A small number of correlations had a p-value lower than 0.01 (see Table 2). We found that IHC staining values of Ki-67 was negatively correlated with std(K^{trans}) and std(v_e), (rho = −0.710; p = 0.004, and rho = −0.726; p = 0.003, respectively). However, the only correlation which was significant after Bonferroni correction for multiple comparisons was the IHC level of VEGF with DCE-MRI parameter std(k_{ep}) (rho = 0.808, p = 0.0001), (see Figure 4). There were no other significant correlations. A non-parametric Mann-Whitney U did not yield significant differences in DCE-MRI, ^{1}H-MRS, or IHC parameters in groups based on HPV status (p>0.28).

Discussion

Untreated HNSCC patients with nodal metastases underwent MRI with ^{1}H-MRS, and DCE-MRI prior to surgery. Surgical specimens were analyzed with immunohistochemistry for several molecular markers. The results of this study revealed statistically significant correlations between measures derived from DCE-MRI and the molecular markers VEGF and Ki-67.

A strong, significant positive correlation was observed between VEGF and std(k_{ep}). Standard deviation measures describing the width of the pixel histogram distribution can be interpreted as being indicative of the tumor heterogeneity.[21] Our results therefore suggest that stimulation of new vessel growth (VEGF) is positively correlated with the heterogeneity measure (std(k_{ep})). This is in keeping with the notion that promotion of angiogenic growth factor pathways also promotes tumor heterogeneity.[24, 25]

Additionally, a strong, significant negative correlation was observed between Ki-67 and heterogeneity markers std(K^{trans}) and std(v_e). This indicates that proliferation of tumor cells is inversely correlated with tumor heterogeneity. This latter observation is in agreement with one of our previous studies, where we imaged 16 HNSCC patients with ^{1}H-MRS, DCE-MRI and ^{18}F-FDG PET before treatment.[11] We observed a strong negative correlation between Cho/W (from ^{1}H-MRS) and std(v_e), which suggested that heterogeneous head and neck tumors contain areas of low proliferation and often highly necrotic regions. In the current study, the number of patients with valid ^{1}H-MRS data was most likely too low to observe a similar trend for Cho/W.

We observed a non-significant negative correlation between VEGF and Ki-67 expression (rho = −0.317, p = 0.27) (see Table 2). Although cell proliferation is an important process that often coincides with angiogenesis during tumorigenesis, there is not a direct one-to-one link between proliferation and angiogenesis.[26] Therefore, the notion that there is a positive correlation of VEGF (i.e. angiogenesis) with tumor heterogeneity, but a negative correlation between Ki-67 (i.e. proliferation) and tumor heterogeneity, is not necessarily conflicting. A previous study by Faratzis et al.,[27] in which immunohistochemical VEGF and Ki-67 expression was investigated in a cohort of 87 patients with SCC of the tongue, did not find a statistical correlation between VEGF and Ki-67 expression.

Human solid tumors are biologically heterogeneous, and display an extensive variation in microvasculature.[25] Measuring the level of heterogeneity of perfusion in tumors can be an important tool for understanding tumor biology or predicting treatment outcome.[25, 28] Several measures of heterogeneity, including standard deviation and skewness, have already been shown to correlate with overall survival, tumor grade or radiation treatment outcome.[14, 29, 30] We recently showed in a DCE-MRI study of 74 patients with HNSCC, that the skewness of K^{trans} was the strongest predictor of progression-free survival and overall survival in HNSCC patients with nodal disease.[14] The exact nature of the tumor heterogeneity in HNSCC is difficult to unravel.[25] A previous HNSCC study attributed the heterogeneity to regions of hypoxia and necrosis within the tumor.[31] The immunohistochemistry necrosis measures in the current study did not correlate with tumor heterogeneity (Table 2), and hypoxia measurements were not obtained. In a previous study, we employed a hypoxia radiotracer FMISO PET/CT and DCE-MRI in patients with HNSCC, and showed that hypoxic nodes had a more asymmetric distribution of k_{ep} values than did non-hypoxic nodes.[12]

It is important to note that some characteristics of the studied MRI and immunohistochemistry techniques are inherently different.[32] Firstly, histology is performed at a much smaller spatial scale (μm) than the voxel size of MRI (mm). Also, accurate registration of histological and MRI planes is not trivial. Finally, *in vitro* immunohistochemistry provides a ‘static’ view, whereas DCE-MRI is a ‘live’ physiologic assay.[33] Therefore, temporal correlation between immunohistochemistry molecular markers and imaging parameters cannot be performed.

Our study has some limitations. The number of patients was low (n=12). Therefore, the observed correlations should be interpreted with caution, and the observed low number of

significant correlations and lack of correlations for CA-IX, HIF-1α, and H&E might be due to the low number of patients. Furthermore, the range of different values for the level of immunostaining for some markers (e.g. HIF-1α) might not be large enough to reach significant correlations. Also, the minimum region of interest that can be studied by ^{1}H-MRS is dependent on the signal-to-noise ratios of the metabolites studied. We studied choline only, as creatine was not visible. Only 7 of the 12 patients had valid ^{1}H-MRS data, and this low number was most likely responsible for the absence of significant correlations found with ^{1}H-MRS. Finally, as indicated above, due to the different spatial scale between MRI and immunohistochemistry, it is difficult to exactly match planes between the two techniques. In the present study, IHC analysis was performed on the nodal tissue and the mucosa as control. Non-metastatic nodes were not used as control, as this tissue was not available. The location of primary tumor in the patients differed considerably (See table 1). A recent study by Tamas et al. [34] revealed that biomarker expression in HNSCC correlates with anatomical localization. More specifically, they studied tissue micro arrays of 124 HNSCC patients which indicated that the level of p16ink4 and Ki67 expression performed immunohistochemical on tissue micro arrays of 124 HNSCC patients and showed a significant elevation of p16(ink4) and Ki67 expression in supraglottic, tonsillar and tonsillo-lingual SCCs compared to SCC of that affecting the oral cavity, oropharynx without tonsils, larynx without supraglottis and the hypopharynx. The diverse biological behavior of the primary tumors in our study needs further investigation.

Regardless of the effect of low patient numbers on correlations not reaching the level of significance, it is also important to note that non-significant correlations should not be regarded as negative results. The observation of a non-significant correlation between an MRI measure and a immunohistochemistry marker could indicate that both techniques are complementary, rather than competitive. Given the different technical natures of the two techniques (different imaging scale and moment), a complementary contribution of both techniques would not be surprising.

The results of this preliminary study indicate that the level of heterogeneity of perfusion in metastatic HNSCC seems positively correlated with angiogenesis, and inversely correlated with proliferation. These results are preliminary in nature and are indicative, and not definitive, trends portrayed in HNSCC patients with nodal disease. Future studies with larger patient populations need to be carried out to validate and clarify our preliminary findings.

Acknowledgments

We thank Ms. Nancy Bennett (M.S.) for editing the manuscript.

Role of the funding source: Supported by NIH National Cancer Institute/National Institutes of Health (grant number 1 R01 CA115895).

Abbreviations

^{1}H-MRS	proton magnetic resonance spectroscopy
CAIX	carbonic anhydrase
Cho	choline
CRLB	Cramer-Rao lower bound
DCE-MRI	dynamic contrast-enhanced magnetic resonance imaging
EES	extravascular extracellular space

HIF-1α	hypoxia inducible transcription factor
HN	head and neck
HNSCC	Head and Neck squamous cell carcinoma
HPV	human papillomavirus
IHC	immunohistochemistry
k_{ep}	rate constant in min^{-1}
K^{trans}	volume transfer constant in min^{-1}
MRI	magnetic resonance imaging
PACS	picture archiving and communication system
PD	proton density
PRESS	point-resolved spatially localized spectroscopy
ppm	parts per million
ROI	region of interest
TE	echo time
TR	repetition time
v_e	volume fraction of the EES
VEGF	vascular endothelial growth factor

References

1. Jemal A, Siegel R, Xu J, Ward E. Cancer statistics, 2010. CA Cancer J Clin. 2010; 60:277–300. [PubMed: 20610543]
2. Leemans CR, Braakhuis BJ, Brakenhoff RH. The molecular biology of head and neck cancer. Nat Rev Cancer. 2011; 11:9–22. [PubMed: 21160525]
3. Shah GV, Wesolowski JR, Ansari SA, Mukherji SK. New directions in head and neck imaging. J Surg Oncol. 2008; 97:644–8. [PubMed: 18493943]
4. Tse GM, King AD, Yu AM, Lam CC, Chan AW, Chen GG, Yeung DK, Yu KH, Bhatia KS, Chan AB. Correlation of biomarkers in head and neck squamous cell carcinoma. Otolaryngol Head Neck Surg. 2010; 143:795–800. [PubMed: 21109080]
5. Hylton N. Dynamic contrast-enhanced magnetic resonance imaging as an imaging biomarker. J Clin Oncol. 2006; 24:3293–8. [PubMed: 16829653]
6. Shah GV, Gandhi D, Mukherji SK. Magnetic resonance spectroscopy of head and neck neoplasms. Top Magn Reson Imaging. 2004; 15:87–94. [PubMed: 15269611]
7. Liu M, Lawson G, Delos M, Jamart J, Chatelain B, Remacle M, Marbaix E. Prognostic value of cell proliferation markers, tumour suppressor proteins and cell adhesion molecules in primary squamous cell carcinoma of the larynx and hypopharynx. Eur Arch Otorhinolaryngol. 2003; 260:28–34. [PubMed: 12520353]
8. Silva SD, Agostini M, Nishimoto IN, Coletta RD, Alves FA, Lopes MA, Kowalski LP, Graner E. Expression of fatty acid synthase, ErbB2 and Ki-67 in head and neck squamous cell carcinoma. A clinicopathological study. Oral Oncol. 2004; 40:688–96. [PubMed: 15172638]
9. Perisanidis C, Perisanidis B, Wrba F, Brandstetter A, El Gazzar S, Papadogeorgakis N, Seemann R, Ewers R, Kyzas PA, Filipits M. Evaluation of immunohistochemical expression of p53, p21, p27, cyclin D1, and Ki67 in oral and oropharyngeal squamous cell carcinoma. Journal of oral pathology & medicine : official publication of the International Association of Oral Pathologists and the American Academy of Oral Pathology. 2011

10. Casado S, Forteza J, Dominguez S, Abad MT, Perez I, Intxaurbe I, del Campo JM, Lopez R. Predictive value of P53, BCL-2, and BAX in advanced head and neck carcinoma. Am J Clin Oncol. 2002; 25:588–90. [PubMed: 12478005]
11. Jansen JF, Schoder H, Lee NY, Stambuk HE, Wang Y, Fury MG, Patel SG, Pfister DG, Shah JP, Koutcher JA, Shukla-Dave A. Tumor Metabolism and Perfusion in Head and Neck Squamous Cell Carcinoma: Pretreatment Multimodality Imaging With (1)H Magnetic Resonance Spectroscopy, Dynamic Contrast-Enhanced MRI, and [(18)F]FDG-PET. Int J Radiat Oncol Biol Phys. 2012; 82:299–307. [PubMed: 21236594]
12. Jansen JF, Schoder H, Lee NY, Wang Y, Pfister DG, Fury MG, Stambuk HE, Humm JL, Koutcher JA, Shukla-Dave A. Noninvasive assessment of tumor microenvironment using dynamic contrast-enhanced magnetic resonance imaging and 18F-fluoromisonidazole positron emission tomography imaging in neck nodal metastases. Int J Radiat Oncol Biol Phys. 2010; 77:1403–10. [PubMed: 19906496]
13. Shukla-Dave A, Lee N, Stambuk H, Wang Y, Huang W, Thaler HT, Patel SG, Shah JP, Koutcher JA. Average arterial input function for quantitative dynamic contrast enhanced magnetic resonance imaging of neck nodal metastases. BMC Med Phys. 2009; 9:4. [PubMed: 19351382]
14. Shukla-Dave A, Lee NY, Jansen JF, Thaler HT, Stambuk HE, Fury MG, Patel SG, Moreira AL, Sherman E, Karimi S, Wang Y, Kraus D, Shah JP, Pfister DG, Koutcher JA. Dynamic Contrast-Enhanced Magnetic Resonance Imaging as a Predictor of Outcome in Head and Neck Squamous Cell Carcinoma Patients with Nodal Metastases. Int J Radiat Oncol Biol Phys. 2011
15. Provencher SW. Estimation of metabolite concentrations from localized in vivo proton NMR spectra. Magn Reson Med. 1993; 30:672–9. [PubMed: 8139448]
16. Provencher SW. LCModel User's Manual. May 5.2009
17. Cavassila S, Deval S, Huegen C, van Ormondt D, Graveron-Demilly D. Cramer-Rao bounds: an evaluation tool for quantitation. NMR Biomed. 2001; 14:278–83. [PubMed: 11410946]
18. Jansen JF, Backes WH, Nicolay K, Kooi ME. 1H MR spectroscopy of the brain: absolute quantification of metabolites. Radiology. 2006; 240:318–32. [PubMed: 16864664]
19. Tofts PS, Brix G, Buckley DL, Evelhoch JL, Henderson E, Knopp MV, Larsson HB, Lee TY, Mayr NA, Parker GJ, Port RE, Taylor J, Weisskoff RM. Estimating kinetic parameters from dynamic contrast-enhanced T(1)-weighted MRI of a diffusable tracer: standardized quantities and symbols. J Magn Reson Imaging. 1999; 10:223–32. [PubMed: 10508281]
20. Parker GJ, Roberts C, Macdonald A, Buonaccorsi GA, Cheung S, Buckley DL, Jackson A, Watson Y, Davies K, Jayson GC. Experimentally-derived functional form for a population-averaged high-temporal-resolution arterial input function for dynamic contrast-enhanced MRI. Magn Reson Med. 2006; 56:993–1000. [PubMed: 17036301]
21. Lee CH, Choi JW, Kim KA, Seo TS, Lee JM, Park CM. Usefulness of standard deviation on the histogram of ultrasound as a quantitative value for hepatic parenchymal echo texture; preliminary study. Ultrasound Med Biol. 2006; 32:1817–26. [PubMed: 17169693]
22. Zhong H, De Marzo AM, Laughner E, Lim M, Hilton DA, Zagzag D, Buechler P, Isaacs WB, Semenza GL, Simons JW. Overexpression of hypoxia-inducible factor 1alpha in common human cancers and their metastases. Cancer Res. 1999; 59:5830–5. [PubMed: 10582706]
23. Cohen, J. Statistical power analysis for the behavioral sciences. 2. Hillsdale, N.J: L. Erlbaum Associates; 1988.
24. Casanovas O, Hicklin DJ, Bergers G, Hanahan D. Drug resistance by evasion of antiangiogenic targeting of VEGF signaling in late-stage pancreatic islet tumors. Cancer cell. 2005; 8:299–309. [PubMed: 16226705]
25. Jackson A, O'Connor JP, Parker GJ, Jayson GC. Imaging tumor vascular heterogeneity and angiogenesis using dynamic contrast-enhanced magnetic resonance imaging. Clin Cancer Res. 2007; 13:3449–59. [PubMed: 17575207]
26. Jansen JF, Koutcher JA, Shukla-Dave A. Non-invasive imaging of angiogenesis in head and neck squamous cell carcinoma. Angiogenesis. 2010; 13:149–60. [PubMed: 20383743]
27. Faratzis G, Tsiambas E, Rapidis AD, Machaira A, Xiromeritis K, Patsouris E. VEGF and ki 67 expression in squamous cell carcinoma of the tongue: An immunohistochemical and computerized image analysis study. Oral Oncol. 2009; 45:584–8. [PubMed: 18804402]

28. Gillies RJ, Schornack PA, Secomb TW, Raghunand N. Causes and effects of heterogeneous perfusion in tumors. Neoplasia. 1999; 1:197–207. [PubMed: 10935474]

29. de Lussanet QG, Backes WH, Griffioen AW, Padhani AR, Baeten CI, van Baardwijk A, Lambin P, Beets GL, van Engelshoven JM, Beets-Tan RG. Dynamic contrast-enhanced magnetic resonance imaging of radiation therapy-induced microcirculation changes in rectal cancer. Int J Radiat Oncol Biol Phys. 2005; 63:1309–15. [PubMed: 16125874]

30. Issa B, Buckley DL, Turnbull LW. Heterogeneity analysis of Gd-DTPA uptake: improvement in breast lesion differentiation. J Comput Assist Tomogr. 1999; 23:615–21. [PubMed: 10433296]

31. Vaupel P. Hypoxia and aggressive tumor phenotype: implications for therapy and prognosis. Oncologist. 2008; 13 (Suppl 3):21–6. [PubMed: 18458121]

32. Atkin G, Taylor NJ, Daley FM, Stirling JJ, Richman P, Glynne-Jones R, d'Arcy JA, Collins DJ, Padhani AR. Dynamic contrast-enhanced magnetic resonance imaging is a poor measure of rectal cancer angiogenesis. The British journal of surgery. 2006; 93:992–1000. [PubMed: 16673354]

33. Gillies RJ, Raghunand N, Karczmar GS, Bhujwalla ZM. MRI of the tumor microenvironment. J Magn Reson Imaging. 2002; 16:430–50. [PubMed: 12353258]

34. Tamas L, Szentkuti G, Eros M, Danos K, Brauswetter D, Szende B, Zsakovics I, Krenacs T. Differential biomarker expression in head and neck cancer correlates with anatomical localization. Pathology oncology research : POR. 2011; 17:721–7. [PubMed: 21487776]

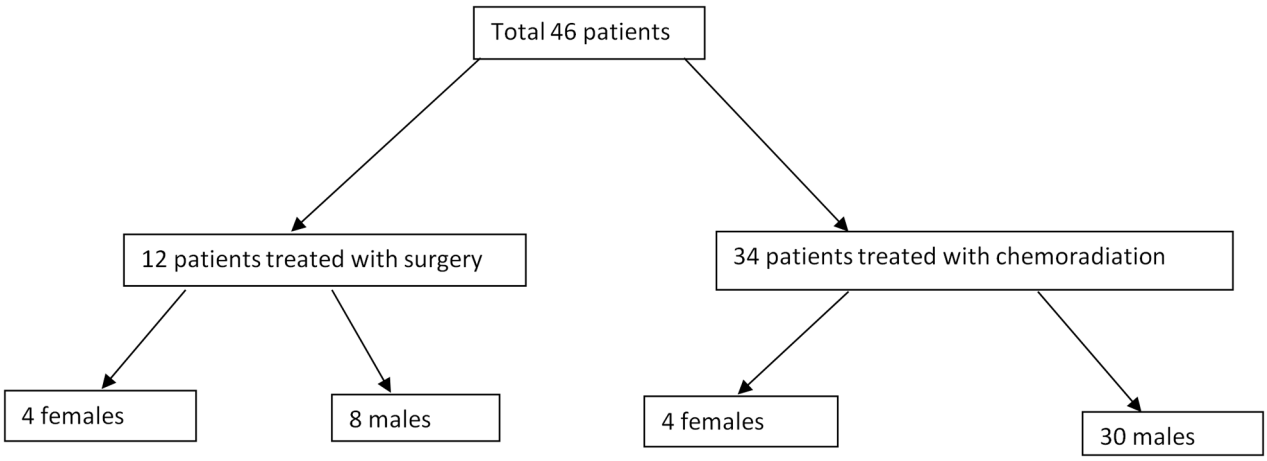

Figure 1.
Flow chart of the patients recruited from March 2006 to March 2008.

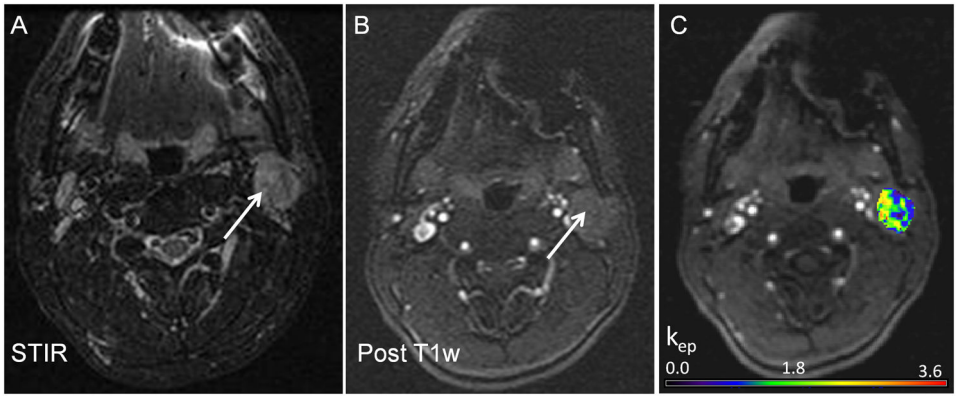

Figure 2.

Figure 2 shows a representative (a) short tau inversion recovery (STIR), (b) a post-contrast T1-weighted, and (c) DCE-MRI parametric k_{ep} map image obtained from the neck region of a HNSCC patient (male, 44 y, primary tonsil).

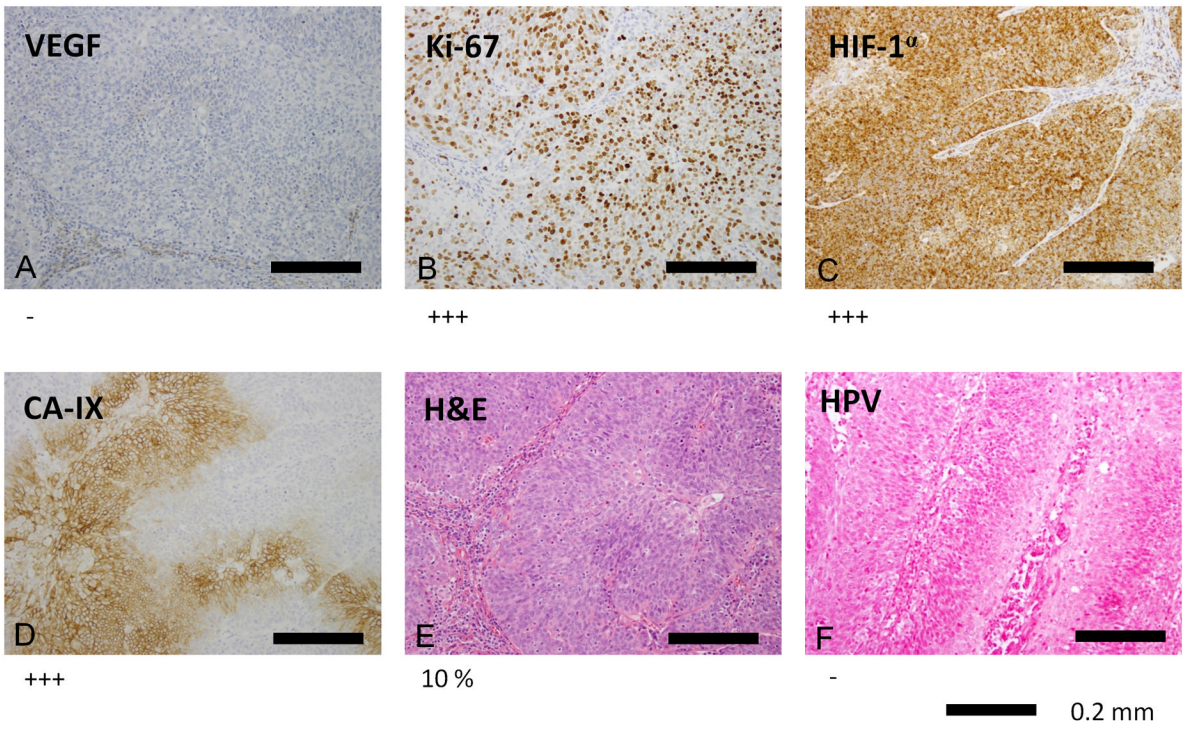

Figure 3.

IHC assay results of the node visualized in Figure 2. (a) VEGF, (b) Ki-67, (c) HIF-1α, (d) CA-IX, (e) H&E, and (f) HPV. The classification is on an ordinal scale: (−) no staining; (+) immunostaining is less than 1% of cells; (++) immunostaining in 1–10% of cells; (+++) immunostaining in 10–50% of cells; (++++) immunostaining in more than 50% of cells. The black bar indicates 0.2 mm.

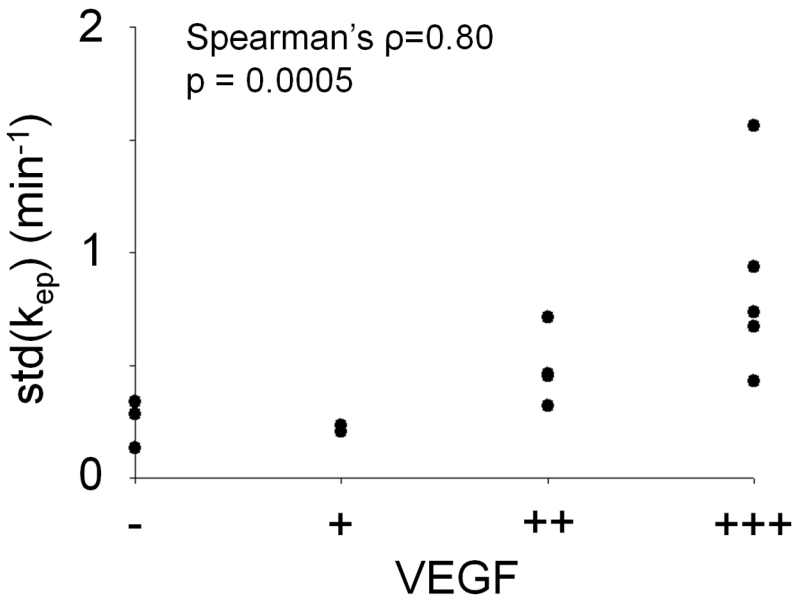

Figure 4.
Scatter plot displaying the relationship between IHC VEGF staining and the DCE-MRI parameter std(k_{ep}).

Table 1

Patient characteristics.

Characteristics	Value
No. of patients	12
Demographics	
Mean age (y)	57
Range (y)	40–79
No. of men	8 (67%)
Location of primary tumor	
Base of tongue	2 (17%)
Tonsil	2 (17%)
Oral Tongue	1 (8%)
Hard Palate	1 (8%)
Buccal Mucosa	2 (17%)
Unknown	4 (33%)
Presenting Stage	
Stage III	1 (8%)
Stage IV	11 (92%)
Number of nodes studied	
1	10 (83%)
2	2 (17%)
Nodal size	
Mean ± SD (mL)	1.2 ± 1.0

Table 2

Spearman rank correlation coefficients for ^{1}H-MRS, DCE-MRI and histological markers.[a,b]

	Cho/W	**median (K^{trans})**	**std (K^{trans})**	**median (ve)**	**std (ve)**	**median (k_{ep})**	**std (k_{ep})**	**VEGF**	**Ki-67**	**CA-IX**	**HIF-1α**	**H&E (necrosis)**
Cho/W	1	−.536	−.786	−.179	−.536	.071	.071	−.487	.597	.231	.299	−.222
median (K^{trans})	-	1	*−.077*	*.727***	*−.451*	*−.433*	*−.662***	−.567	.182	.268	.430	−.313
std (K^{trans})	-	-	1	*−.046*	*.710***	*.165*	*.446*	.528	**−.710****	.123	−.390	−.378
median (ve)	-	-	-	1	*−.288*	*−.877***	*−.798***	−.615	.068	−.109	.090	−.233
std (ve)	-	-	-	-	1	*.156*	*.644*	.638	**−.726****	.000	−.325	−.193
median (k_{ep})	-	-	-	-	-	1	*.705***	.496	−.013	.398	.023	−.027
std (k_{ep})	-	-	-	-	-	-	1	**.808*****	−.429	.188	−.120	−.024
VEGF	-	-	-	-	-	-	-	1	−.317	.162	−.306	−.016
Ki-67	-	-	-	-	-	-	-	-	1	−.077	.025	.210
CA-IX	-	-	-	-	-	-	-	-	-	1	.527	−.571
HIF-1α	-	-	-	-	-	-	-	-	-	-	1	.067
H&E (necrosis)	-	-	-	-	-	-	-	-	-	-	-	1

[a] Cho/W = choline concentration; std = standard deviation; K^{trans} = volume transfer constant; v_e = extravascular extracellular volume fraction; k_{ep} = redistribution rate constant; VEGF = vascular endothelial growth factor; Ki-67 reflects cellular proliferation; CAIX = carbonic anhydrase; HIF-1α = hypoxia inducible transcription; and H&E = hematoxylin-eosin.

[b] Intra-modality and significant inter-modality and correlation coefficients are printed in '*grey italic*' and '**bold**', respectively.

** $p < 0.01$

*** $p < 0.01$, corrected for multiple comparisons (Bonferroni)